Atmos. Chem. Phys. Discuss., 8, 12197–12225, 2008
www.atmos-chem-phys-discuss.net/8/12197/2008/

Atmospheric Chemistry and Physics Discussions

Mechanisms for synoptic transport of atmospheric CO_2 in the midlatitudes and tropics

N. Parazoo[1], A. Denning[1], S. Kawa[2], K. Corbin[1], R. Lokupitiya[1], and I. Baker[1]

[1]Atmospheric Science Department, Colorado State University, Fort Collins, Colorado, USA
[2]NASA Goddard Space Flight Center, Greenbelt, Maryland, USA

Received: 15 April 2008 – Accepted: 28 May 2008 – Published: 20 June 2008

Correspondence to: N. Parazoo (nparazoo@atmos.colostate.edu)

Published by Copernicus Publications on behalf of the European Geosciences Union.

Abstract

Synoptic variations of CO_2 mixing ratio produced by interactions between weather and surface fluxes are investigated mechanistically and quantitatively in midlatitude and tropical regions using continuous in-situ CO_2 observations in North America, South America and Europe and forward chemical transport model simulations with the Parameterized Chemistry Transport Model. Frontal CO_2 climatologies show consistently strong, characteristic frontal CO_2 signals throughout the midlatitudes of North America and Europe. Transitions between synoptically identifiable CO_2 air masses or transient spikes along the frontal boundary typically characterize these signals. One case study of a summer cold front shows that CO_2 gradients organize with deformational flow along weather fronts producing strong and spatially coherent variations. A boundary layer budget equation is constructed in order to determine contributions to boundary layer CO_2 tendencies by horizontal and vertical advection, moist convection, and biological and anthropogenic surface fluxes. Analysis of this equation suggests that, in midlatitudes, advection is responsible for 50–90% of the amplitude of frontal variations in the summer, depending on upstream influences, and 50% of all day-to-day variations throughout the year. Simulations testing sensitivity to local cloud and surface fluxes further suggest that horizontal advection is a major source of CO_2 variability in midlatitudes. In the tropics, coupling between convective transport and surface CO_2 flux is most important. Due to the scarcity of tropical observations available at the time of this study, future work should extend such mechanistic analysis to additional tropical locations.

1 Introduction

Continuous in-situ measurements of atmospheric CO_2 over midlatitude and tropical regions exhibit synoptic variations strongly influenced by coupling between weather and surface CO_2 flux (e.g. Law et al., 2002; Gerbig et al., 2003; Geels et al., 2004; Lin

et al., 2004). Weather differences in the midlatitudes and tropics can be explained in part by the different energy reserves available in the atmosphere. In the tropics, latent heat release associated with cumulus convection is the significant source of energy for weather (Holton, 1992). Although latent heat is important in midlatitudes, it is generally thought to be a secondary energy source for synoptic weather. Midlatitude synoptic scale weather disturbances derive energy from the zonal available potential energy associated with latitudinal temperature gradients (baroclinicity). In the tropics, because of weak temperature gradients and negligible Coriolis, baroclinic effects are weak. Due to energy constraints, horizontal mixing is more prevalent in midlatitudes while vertical convective mixing is more prevalent in the tropics.

Figure 1 shows midday planetary boundary layer (PBL) CO_2 (given as a mole fraction in units of parts per million (ppm)), from sites in North America, South America and Europe, where midday maximizes the amount regional and synoptic influence compared to local influence during well-mixed boundary layer conditions (Bakwin et al., 1998). Synoptic variations of 10–20 ppm over 1–3 days are common, comparable to seasonal amplitudes. Continental variations under terrestrial influence are typically much stronger than in remote mountainous and maritime locations. A comparison of monthly standard deviation of midday values at continental (e.g. LEF, HRV, and HEI) and remote (e.g. MLO, BRW, and ZEP) sites verifies this (Fig. 1).

Davis et al. (2003) observed that daily PBL CO_2 tendencies at a site in Northern Wisconsin are governed primarily by local net ecosystem exchange (NEE, defined as gross primary production minus ground respiration) during fair weather. During May and September, however, the sign of NEE was contradictory to CO_2 tendencies expected from NEE of CO_2. Preliminary investigation explained this through the presence of discrete non-fair weather events such as frontal passage. Whether the source for such variations was horizontal or vertical advection could not be explained.

In non-fair weather events, such as surface cold fronts, mechanisms for synoptic variations that have been proposed in the literature include: 1) nonlocal influence through lateral advection of upstream horizontal CO_2 gradients, 2) vertical motion through moist

convection and frontal lifting over air mass boundaries along frontal zones, and 3) ecosystem respiration and photosynthesis response to frontal weather. Several studies (e.g. Worthy et al., 2003; Chan et al., 2004; Geels et al., 2004; Corbin and Denning, 2006) have investigated the role of horizontal advection. These studies conclude that horizontal advection of remotely generated CO_2 anomalies is an important source for downstream variations. Chan et al. (2004) also found that biospheric fluxes are strongly coupled to radiative forcing changes under cloud cover associated with fronts.

This study investigates and quantifies mechanisms responsible for synoptic variations in midlatitudes and the tropics using well-calibrated continuous observations from 17 sites across the globe, global transport model simulations, and boundary layer budget analysis. The remainder of the paper is organized as follows: Sect. 2 describes the simulation models and CO_2 observations, Sect. 3 discusses the observed and simulated midlatitude and tropical synoptic variations, and Sect. 4 summarizes results.

2 Methods

2.1 Observations

Continuous CO_2 observations are utilized in this study to investigate variations continuously in time at a point in space. These data were collected from well-calibrated continuous stations in North America, South America, and Europe. Midday values (the mixing ratio averaged from 1–5 pm local time) were used from hourly time series to investigate day-to-day variability. Although the range of measurement heights varies from 9–457 m a.g.l., only measurements between 9–40 m were included in the analysis for consistency. The use of midday values ensures that the boundary layer is well mixed such that CO_2 values near the surface and those near the top of the PBL have similar mixing ratios. This also helps to maximize comparison to transport simulations, which struggle to capture concentrations during stable periods. Figure 2 shows the location of each site. Table 1 gives a brief description of each site. Descriptions

of the majority of these sites can also be found at http://www.esrl.noaa.gov/gmd/ and http://gaw.kishou.go.jp/wdcgg/.

2.2 Models and driver data

The Parameterized Chemistry Transport Model (PCTM) was used for forward global simulations of CO_2 transport (e.g. Kawa et al., 2004). This provides a diagnostic tool for studying synoptic interactions among weather and surface CO_2 flux. Transport fields were provided by NASA's Goddard Earth Observation System, version 4 (GEOS4), data assimilation system (GEOS4-DAS) (Bloom et al., 2005) and include 6-hourly analyzed winds, temperatures, diffusion coefficients, and convective mass fluxes. Physical parameterizations are derived from the National Center for Atmospheric Research Community Climate Model, Version 3 (Kiehl et al., 1998). Subgrid scale vertical processes include cumulus convection (cloud mass flux (CMF) from deep (Zhang and McFarlane, 1995) and shallow (Hack et al., 1994) parameterized convection) and turbulence parameters. Surface CO_2 fluxes include hourly NEE from the Simple Biosphere Model, Version 3 (SiB3), constant in time anthropogenic fossil fuel emissions (FF) (Andres et al., 1996), and monthly air-sea exchange (OCEAN) of CO_2 (Takahashi et al., 2002). Fire emissions are ignored.

SiB is a land-surface parameterization scheme originally used to simulate biophysical processes in climate models (Sellers et al., 1986), but later adapted to include ecosystem metabolism (Sellers et al., 1996a; Denning et al., 1996). SiB involves the direct calculation of carbon assimilation by photosynthesis to calculate land-atmosphere CO_2 exchange (Denning et al., 1996; Sellers et al., 1996a). The soil representation is similar to that of CLM (Dai et al., 2003), with 10 soil layers and an initial soil column depth of 3.5 m. SiB has been updated to include prognostic calculation of temperature, moisture, and trace gases in the canopy air space, and the model has been evaluated against eddy covariance measurements at a number of sites (Baker et al., 2003; Hanan et al., 2005; Vidale and Stockli, 2005). We refer to this base version of the code as SiB3.

SiB3 was run in steady state mode in which ecosystem respiration balances gross primary production over one year at every grid point. The meridional gradient and secular trends simulated by the model are therefore stronger than observed (Kawa et al., 2004), but we focus on synoptic time scales. Flux and energy calculations in SiB3 were driven by GEOS4-DAS meteorology. GEOS4 precipitation was scaled by monthly precipitation from the Global Precipitation Climatology Project (GPCP) (Huffman et al., 2001) to force total monthly precipitation in GEOS4 to match that of GPCP. The time at which precipitation occurs remained unchanged so that covariance of anomalies in cloudiness, moisture, and vertical transport is conserved.

Details of PCTM and the experimental setup are similar to Kawa et al. (2004). PCTM was run from 2000–2004 at 1.25° by 1° (longitude by latitude) with 25 levels to 1 mbar, where 2000–2002 comprised the spin up period to establish the interhemispheric CO_2 gradient.

3 Discussion

3.1 Frontal CO_2

As discussed in Sect. 1, discrete frontal passage events in the spring and autumn can cause CO_2 mixing ratios that are inconsistent with the sign of local NEE. Frontal systems, however, occur all year in midlatitudes, and may therefore be responsible for causing variations regardless of local surface fluxes. We can start thinking about the role of cold fronts in redistributing CO_2 throughout the atmosphere by briefly discussing cold front dynamics. Fronts are a result of baroclinicity, in which differential solar heating between the equator and pole brings about meridional temperature gradients that tend to concentrate in baroclinic zones associated with tropospheric jet streams. Through instabilities, baroclinic waves can then remove available potential energy from the mean flow and provide energy for the development of synoptic scale storms, such as cold fronts, which act to reduce horizontal temperature gradients by mixing thermo-

dynamically unique air masses; i.e. transporting relative cold dry air south and warm moist air north.

By analyzing CO_2 mixing ratio signals during frontal passage over multiple frontal events and averaging the signals together, we find that cold fronts are indeed important for producing strong downstream variations and, furthermore, that these variations are persistent throughout the year. Figure 3 shows climatologies of simulated and observed growing season (June–September) frontal CO_2 events at continuous sites in North America and Europe. Winter climatologies (December–February) are shown in Fig. 4.

The procedure for creating these climatologies is as follows. First, some general way of defining frontal zones in which frontal signals occur is needed. This study focuses on surface-based cold fronts in part because their surface signatures tend to be more sharply defined than other surface fronts, making them easier to identify and study (Schultz, 2005). We characterize surface fronts according to the Clarke and Renard (1965) definition, who define a front as "the warm-air boundary of a synoptic-scale baroclinic zone of distinct thermal gradient... Further, the frontal-zone boundaries are considered as quasi first-order thermal and moisture discontinuities." Temporal gradients of temperature and water vapor are used together with clockwise wind shifts and pressure minima to locate the warm-air boundary. Other frontal weather fields such as precipitation and radiation were not used to classify fronts. Although important for NEE (Chan et al., 2004) such classification was beyond the scope of this study.

Surface pressure and 10 m wind, temperature, and specific humidity from GEOS4-DAS were used to identify the time of frontal passage at all of the continuous CO_2 sites. The long-term trend and diurnal/seasonal cycles were removed from the temperature and specific humidity time series using a butterworth filter until only synoptic variations remained, which we define to occur at a frequency range of 1–10 days. Frontal passage was then approximated as the time at which the second order gradients in specific humidity and temperature were at their maxima over the synoptic time scale (1–5 days), concurrent with a clockwise wind shift and approximate pressure minima. Since only

3-hourly reanalysis was available for this analysis, all times are approximate. Figure 5, which shows the summer climatology (averaging procedure discussed below) of the observed and simulated meteorology at three sites in North America, demonstrates that the timing of fronts identified in the reanalysis are consistent with observations.

After identifying particular events, the long-term trend and diurnal/seasonal cycles were removed from observed hourly and simulated 3-hourly CO_2 time series. Frontal composites were constructed by averaging synoptic anomalies at each station from 48 h before frontal passage until 48 h after. The result is the average frontal signal that the station observes (and simulates) as the front passes by. The signals in Figs. 3 and 4 vary with time at a point in space defined by the station, where time increases on the x-axis from left to right with zero representing the time of frontal passage and negative (positive) time anomalies representing the signal before (after) frontal passage.

Focusing for now on the growing season, frontal climatologies suggest that some sites (e.g. SGP, WKT, SBI, and WPL) feature air mass replacement of higher prefrontal CO_2 with lower postfrontal CO_2. At other sites CO_2 variations occur as transient spikes during frontal passage (e.g. CDL, AMT, and ZEP). The top and middle plots of Fig. 6, which show July mean NEE and FF over North America, combined with the frontal identification constraint discussed earlier that all frontal events used in the frontal climatologies exhibit clockwise wind shifts characteristic of cold fronts in which the wind is generally from the south prior to frontal passage and from the north afterwards, helps to explain the nature of these signals and why they vary between sites. When maps of NEE, FF, and OCEAN are combined into the time mean (bottom plot of Fig. 6) we find a quite diverse pattern of influence unique to each site (site location plotted for convenience).

SGP and WKT, for example, exhibit a frontal signal in which CO_2 mixing ratios decrease over the course of frontal passage. According to Fig. 6, the region containing these sites is dominated by positive surface flux while the region to the north is dominated by negative surface flux. This creates a north-south gradient in surface flux which, when under the influence of fair weather typical of a high-pressure system, is

expected to create relatively CO_2 depleted air masses to the north and CO_2 enriched air masses to the south. If air is then advected from the north as a low-pressure system settles in and frontal passage ensues, as might be expected due to typical wind patterns associated with fronts, this would help to explain the decreasing CO_2 tendency associated with frontal signals observed at SGP and WKT. Such unique upstream surface flux influences (each site is different), combined with horizontal advection along cold fronts (see Sect. 3.2), help to interpret these frontal CO_2 signals.

3.2 Budget analysis

Since PCTM reproduces much of the amplitude, shape, and phase of the observed composite surface signals in Figs. 3 and 4, we turn to an analysis of model output to study physical and biological mechanisms active along fronts to determine the role of advection in the frontal CO_2 signatures discussed above. Diagnosis of simulated advective tendencies associated with frontal climatologies illustrates the importance of advection compared to surface flux and moist convection during frontal passage.

$$\underbrace{\frac{\partial C}{\partial t}}_{\text{i}} + \underbrace{\frac{RT}{p}\frac{F_c}{z_1}}_{\text{ii}} + \underbrace{K_m\frac{\partial C}{\partial z}}_{\text{iii}} + \underbrace{W\frac{\partial C}{\partial z}}_{\text{iv}} + \boldsymbol{V_H}\cdot\boldsymbol{\nabla}_H C_\mathrm{v} + \underbrace{g\frac{M\partial C}{\partial p}}_{\text{vi}} = 0 \quad (1)$$

Equation (1) represents the simulated CO_2 tendency (i) due to surface flux (ii), vertical diffusion (iii), vertical advection (iv), horizontal advection (v), and vertical cloud transport, where C is CO_2 mixing ratio in ppm, F_c is the surface flux due to NEE, FF, and OCEAN, z_1 is the lowest model level (~50 m), R is the gas constant, T is temperature, p is pressure, K_m is the vertical diffusion coefficient, W is vertical velocity, $\boldsymbol{V_H}$ is the horizontal wind, g is gravity, and M is net convective mass flux as described in the work of Kawa et al. (2004).

To gauge relative importance, each term was output from PCTM every hour (terms (ii) and (iii) together represent vertical diffusion of surface flux). Hourly tendencies at each layer within the PBL were averaged through the three lowest model levels and

then converted to daily averaged tendencies, where level three (approximately 500 m above the surface) is assumed to represent the PBL height at all times such that the dominance of shallow nocturnal PBL's on surface flux tendencies is reduced. The resulting terms represent synoptic PBL CO_2 tendencies. The sum of the advective tendencies were divided by the sum of all tendencies, and then averaged across the same events used in the frontal climatologies, to represent the fractional contribution of advection to frontal CO_2 variations (dashed lines in Figs. 3 and 4).

An example of annual mean percent contributions at several sites in North and South America are shown in Table 2. These values are discussed in Sect. 3.3. For now discussion is limited to frontal events. This method suggests that daily average advective contribution is approximately 60% during frontal passage in the summer, ranging from about 30% where local surface flux (NEE+FF) tendencies dominate (e.g. FRS and PAL) to above 75% where advection dominates (islands like MHD, ZEP and SBI and remote regions like BRW and ALT). Vertical cloud transport accounts for about 8% of frontal CO_2 tendencies on average. Advection accounts for a larger percentage in the winter (69%) when NEE is weaker.

3.3 Deformational flow

Transient variations associated with frontal passages are interpreted in a case study of a simulated low-pressure system near FRS. Figure 7 shows daily snapshots of surface CO_2 and wind vectors in the days leading up to a spike at FRS. In this example, several positive CO_2 anomalies (SW quadrant of 7a and 7b) have formed ahead of the developing cyclone (NW quadrant of 7b) due, in this case, to persistent positive NEE and advection of FF generated anomalies from the east (not shown). The anomalies merge together in the wind shear south of the cyclone. On day 3 (7c) the anomalies become aligned with the front and advect to the east during day 4 (7d). The preexisting NE-SW CO_2 gradient was organized and concentrated into a narrow frontal zone of high CO_2 by deformational flow.

Deformational flow is the basis for the theory presented in this paper to explain the or-

ganization of CO_2 along cold fronts, which, through converging and shearing wind fields along frontal boundaries, acts to stretch and shear tracers in the flow. Holton (1992) used kinematic theory and an equation similar to Eq. (2):

$$\frac{D_g}{Dt}\left(\frac{\partial C}{\partial x}+\frac{\partial C}{\partial y}\right) = -\underbrace{\frac{\partial u_g}{\partial x}\frac{\partial C}{\partial x}}_{\text{I}} - \underbrace{\frac{\partial v_g}{\partial x}\frac{\partial C}{\partial y}}_{\text{II}} - \underbrace{\frac{\partial u_g}{\partial y}\frac{\partial C}{\partial x}}_{\text{III}} - \underbrace{\frac{\partial v_g}{\partial y}\frac{\partial C}{\partial y}}_{\text{IV}} \quad (2)$$

to explain the effect of deformational forces of passive tracers. When the total geostrophic tendency (D_g/Dt) is applied to a horizontal plane of CO_2 (C), and assuming geostrophic winds (u_g and v_g) and no vertical motion, shear deformation (terms II and III) rotates parcels through shear vorticity, concentrating CO_2 gradients along lines of maximum shear (e.g. the strong shear zone south of low-pressure center in 7c), while stretching deformation (terms I and IV) deforms tracers fields through stretching parallel to the shear vector such that CO_2 concentrates along the axis of dilation (e.g. along the cold front in 7c, d).

In the example above, deformational forces acted to enhance CO_2 gradients along the frontal zone and, together with the traveling cyclone-front system, helped create important downstream variations. Converging wind fields are common along fronts, enhanced by frontogenesis, although the full extent of frontogenetic dynamics are not likely to be captured in the coarse resolution of the GCM used to create the transport fields of GEOS4-DAS. Nevertheless, this example demonstrates the importance of fronts, through deformation flow and advection, for transporting remotely generated CO_2 anomalies, enhancing gradients, and causing variations that are non-local to sites thousands of kilometers away, and helps to explain the strong transient CO_2 variations shown in Figs. 3 and 4 and the importance of advection during frontal passage discussed in terms of the budget analysis.

Furthermore, cloudiness and precipitation are common along frontal transition zones. With the above evidence that CO_2 anomalies concentrate along this same zone, this presents a potential problem for satellite observations of column CO_2 because

frontal anomalies are likely to be hidden under clouds (Corbin and Denning, 2006). Surface observations, which measure continuously in time, are more effective for recording boundary layer variations along fronts. Continuous surface observations are therefore complementary to satellite observations, which observe much more continuously in space.

In the analysis above, 60% of midlatitude frontal variations were attributed to horizontal and vertical transport through air mass exchange and deformational flow. This is not so for the tropics, where baroclinic disturbance is less prevalent, yet CO_2 variations during the rainy season are as large as midlatitude variations, suggesting the presence of other sources for variability. Mechanisms for tropical variations are analyzed below.

3.4 Midlatitude vs tropical mechanisms

Sensitivity of tropical and midlatitudes PBL CO_2 to local and regional processes is tested with simple modeling experiments. For the control run (CONTROL), PCTM was employed as described in Sect. 2. In two sensitivity experiments, 10° square domains are defined centered at grid cells in the tropics (TPJ: 3° S, 55° W) and in midlatitudes (CDL: 54° N, 105° W, SGP: 37° N, 97.5° W, and AMT: 45° N, 69° W). The domains are shown in Fig. 8. In the first experiment (NOCLOUD) sensitivity to moist convective transport was assessed by running PCTM for one year with CMF set to zero in these domains. Cloud-radiative NEE forcing still occurs offline in SiB3, but CMF transport in PCTM does not. In the second experiment (NOFLUX), CMF is retained but NEE and FF surface fluxes are set to zero in the same 10° domains.

We must define and justify some terminology before proceeding. The four budget terms of interest for this analysis are: horizontal advection, vertical advection, cloud transport, and surface flux, as described in Sect. 3.2. We define non-local dynamics to be regional synoptic processes acting on the 10° domains that help to cause variations at the designated sites within these domains. These terms include horizontal and vertical advection, which are controlled by synoptic meteorology and act to transport CO_2 anomalies laterally and vertically. Local dynamics are defined to be mesoscale

processes that act within the 10° domains and cause variations local to one grid cell. These include moist convection and surface flux.

Figure 9 (top row) shows monthly standard deviations of midday observed and simulated CO_2 for each site and run. NOFLUX causes standard deviations to decrease relative to CONTROL at each site, but by a much larger percentage in the tropics such that local variations are greatly reduced. In NOCLOUD, variations are insensitive to moist convection at AMT and CDL, mildly sensitive at SGP, and strongly sensitive at TPJ. These simulations suggest tropical variations are more sensitive to local surface flux and moist convection than in midlatitudes. Despite excluding local surface flux in one experiment and moist convection in the other, strong midlatitude variations are retained in both cases, implying that the advection terms are creating variations in the absence of local processes. The bottom row of Fig. 9, which shows monthly standard deviations of budget advection and cloud transport (as described earlier) for CONTROL, demonstrates that horizontal CO_2 advection contributes more to variability in midlatitudes than does moist convective transport, but that moist convection contributes more than horizontal advection in our one tropical case. Table 2 quantifies percent contributions from individual terms of the budget equation at each of these sites for an entire year. This illustrates the discrepancy between the midlatitudes and tropics in total advection (vertical+horizontal), cloud transport, and surface flux, with advection weaker and surface flux and cloud transport stronger in the tropics.

These experiments suggest different physical controls on day-to-day CO_2 variations in the midlatitudes and tropics. Important controls in midlatitudes are local (surface flux is 52% on average at the three North American sites) and non-local (horizontal and vertical advection combined account for 46% on average), with cloud transportmoist convection contributing only 3% on average. Tropical variations, on the other hand, appear to be more strongly sensitive to local processes in which clouds (11% of total) and surface flux (74%) dominate over advection (15%) in the annual budget. These tropical budget contributions are suggestive of a coupling of local processes where PBL CO_2 recharges from surface fluxes and discharges vertically through convective

transport. The simulations suggest that this may be particularly true during the wet season (~December–April), where simulated NEE is typically positive (Baker et al., 2008). We find that simulated CO_2 variability more than doubles in NOCLOUD and is strongly damped in NOFLUX. These simulations also suggest that regional transport in the tropics must be occurring frequently enough to prevent boundless CO_2 growth in NOCLOUD.

We find that variations in the tropics are just as large as those in midlatitudes but caused for different reasons. Synoptic variations in the tropics appear to be sensitive to a coupling of surface flux and moist convective transport. The importance of convective transport implies that much of the CO_2 anomalies created within the boundary layer are transported to the upper troposphere by moist convection and hidden from surface towers, and, with regard to inverse modeling, need to be accounted for either with proper modeling techniques and/or through upper air CO_2 observations.

4 Summary and conclusions

Continuous in-situ observations in North America, South America, and Europe suggest that strong synoptic variations occur year round, but atmospheric circulation differences cause different primary mechanisms for variations in midlatitude and tropical regions. Analysis of observed and simulated summer frontal CO_2 climatologies show that cold fronts are important for large scale mixing and local midlatitude synoptic variations. A frontal case study suggests that deformational flow along fronts tends to create and maintain anomalous CO_2 signals from the surrounding environment, and that these anomalies can then advect along with fronts as they migrate across the continent. Furthermore, these frontal anomalies are likely to be hidden under clouds due to moist convection associated with fronts. Well-calibrated, in-situ continuous continental CO_2 measurements are, therefore, a required complement to satellite observations.

Because of fundamental differences in atmospheric circulation in the tropics and midlatitudes, this study sought out to understand and quantify physical and biological

mechanisms in the midlatitudes and tropics responsible for strong observed synoptic CO_2 variations in the two regions. Boundary layer budget analysis, combined with cloud and surface flux sensitivity experiments, suggest that regional advective processes, including those associated with fronts, are major sources for synoptic CO_2 variability in midlatitudes, whereas strong coupling between convective transport and surface CO_2 flux is most important in the tropics, where baroclinically induced synoptic transport is much weaker. With more continuous CO_2 observations becoming available in the tropics, future work should extend the mechanistic analysis to additional tropical locations.

Acknowledgements. This research would not been possible without data providers. We thank Margaret Torn, Sebastien Biraud, and Marc Fischer at LBNL for SGP, William Munger and Steve Wofsy at Harvard University for HRV and TPJ, Arlyn Andrews at NOAA/ESRL/GMD for LEF, WKT, and AMT, Douglas Worthy at MSC for CDL, FRS, ALT, and SBI, Larry Flanagan at the University of Lethbridge for WPL, Philippe Ciais and Leonard Rivier for their work in the Carboeurope Database, Johan Strom at SU for ZEP, Tuula Aalto at FMI for PAL, Ingeborg Levin at UHEI-IUP for HEI, Michel Ramonet at CEA-LSCE for MHD, Laszlo Haszpra and Zoltan Barcza for HUN, and WMO WDCGG and NOAA/ESRL/GMD for making CO_2 data publicly available. This research is supported by the National Aeronautics and Space Administration Contracts #NNX06AC75G, #NNG05GD15G, and #NNG06GB41G.

References

Andres, R. J., Marland,G., Fung, I., and Matthews, E.: A 1 degrees × 1 degrees distribution of carbon dioxide emissions from fossil fuel consumption and cement manufacture, 1950–1990, Global Biogeochem. Cy., 10, 419–429, 1996.

Baker, I. T., Denning, A. S., Hanan, N., Prihodko, L., Vidale, P.-L. Davis, K., and Bakwin, P.: Simulated and observed fluxes of sensible and latent heat and CO_2 at the WLEF-TV Tower using SiB2.5, Global Change Biol., 9, 1262–1277, 2003.

Baker, I. T., Prihodko,L., Denning, S., Goulden, M., Miller, S., and Da Rocha, H. R.: Seasonal Drought Stress in the Amazon: Reconciling Models and Observations, J. Geophys. Res., doi:10.1029/2007JG000644, 2008, in press.

Bloom, S., da Silva, A., and Dee, D.: Documentation and Validation of the Goddard Earth Observing System (GEOS) Data Assimilation System, Version 4. Technical Report Series on Global Modeling and Data Assimilation, 2005.

Chan, D., Yuen, C. W., Higuchi, K., Shashkov, A., Liu, J., Chen, J., and Worthy, D.: On the CO_2 exchange between the atmosphere and the biosphere: the role of synoptic and mesoscale processes, Tellus, 56B, 194–212, 2004.

Clarke, L. C. and Renard, R. J.: Experiments in numerical objective frontal analysis, Mon. Weather Rev., 93, 547–556, 1965.

Corbin, K. D., Denning, A. S.: Using continuous data to estimate clear-sky errors in inversion of satellite CO_2 measurements, Geophys. Res. Lett., 33, LI2810, doi:10.1029/2006GL025910, 2006.

Dai, Y., Zeng, X., Dickinson, R. E., Baker, I., Bonan, G., Bosilovich, M., Denning, S., Dirmeyer, P., Houser, P., Niu, G., Oleson,K., Schlosser,A., and Yang, Z.-L.: The common land model, B. Am. Meteorol. Soc., 84, 1013–1023, 2003.

Davis, K. J., Bakwin, P. S., Yi, C., Berger, B. W., Zhao, C., Teclaw, R. M., and Isebrands, J. G.: The annual cycle of CO_2 and H_2O exchange over a northern mixed forest as observed from a very tall tower, Global Change Biol., 9, 1278–1293, 2003.

Denning, A. S., Collatz, J. G., Zhang, C., Randall, D. A., Berry, J. A., et al: Simulations of terrestrial carbon metabolism and atmospheric CO_2 in a general circulation model. Part 1: Surface carbon fluxes, Tellus, 48B, 521–542, 1996a.

Gamnitzer, U., Karstens, U., Kromer, B., Neubert, R. E. M., Meijer, H. A. J., Schroeder, H., and Levin, I.: Carbon monoxide: A quantitative tracer for fossil fuel CO_2, J. Geophys. Res., 111, D22302, doi:10.1029/2005JD006966, 2006.

Geels, C., Doney, S. C., Dargaville, R., Brandt, J., and Christensen, J. H.: Investigating the sources of synoptic variability in atmospheric CO_2 measurements over the Northern Hemisphere continents: a regional model study, Tellus, 56B, 35–50, 2004.

Gerbig, C., Lin, J. C., Wofsy, S. C., Daube, B. C., Andrews, A. E., Stephens, B. B., Bakwin, P. S., and Grainger, C. A.: Toward constraining regional-scale fluxes of CO_2 with atmospheric observations over a continent: 2. Analysis of COBRA data using a receptor-oriented framework, J. Geophys. Res., 108(D24), 4757, doi:10.1029/2003JD003770, 2003.

Hack, J. J.: Parameterization of moist convection in the National Center for Atmospheric Research community climate model (CCM2), J. Geophys. Res., 99, 5551–5568, 1994.

Hanan, N. P., Berry, J. A., Verma, S. B., Walter-Shea, E. A., Suyker, A. E., Burba, G. G., and

Denning, A. Scott: Testing a model of CO_2, water and energy exchange in Great Plains tall-grass prairie and wheat ecosystems, Agricultural and Forest Meteorology, 131, 162–179, 2005.

Haszpra, L., Barcza, Z., Bakwin, P. S., Berger, B. W., Davis, K. J., and Weidinger, T.: Measuring system for the long-term monitoring of biosphere/atmosphere exchange of carbon dioxide, J. Geophys. Res., 106D, 3057–3070, 2001.

Holton, J. R.: An Introduction to Dynamic Meteorology, Third Edition, Elsevier, San Diego, CA, 1992.

Huffman, G. J., Adler, R. F., Morrissey, M., Bolvin, D. T., Curtis, S., Joyce, R., McGavock, B., and Susskind, J.: Global Precipitation at One Degree Daily Resolution from Multi-Satellite Observations, J. Hydrometeor, 2, 36–50, 2001.

Law, R. M., Rayner, P. J., Steele, L. P., and Enting, I. G.: Using high temporal frequency data for CO2 inversions, Global Biogeochem. Cy., 16(4), 1053, doi:10.1029/2001GB001593, 2002.

Kawa, S. R., Erickson III, D. J., Pawson,S., and Zhu, Z.: Global CO_2 transport simulations using meteorological data from the NASA data assimilation system, J. Geophys. Res., 109, D18312, doi:10.1029/2004JD004554, 2004.

Kiehl, J. T., Hack,J. J., Bonan, G. B., Boville, B. A., Williamson, D. L., and Rasch, P. J.: The National Center for Atmospheric Research Community Climate Model: CCM3, J. Climate, 11, 1131–1149, 1998.

Lin, J. C., Gerbig, C., Wofsy, S. C., Andrews ,A. E., Daube, B. C., Grainger, C. A., Stephens, B. B., Bakwin, P. S., and Hollinger, D. Y.: Measuring fluxes of trace gases at regional scales by Lagrangian observations: Application to the CO2 Budget and Rectification Airborne (CO-BRA) study, J. Geophys. Res., 109, D15304, doi:10.1029/2004JD004754, 2004.

Schultz, D. M.: A review of cold fronts with prefrontal troughs and wind shifts, Mon. Weather Rev., 133, 8, 2449–2472, 2005.

Sellers, P. J., Mint Z. Y., Sud, Y. C., Dalcher,A.: A simple biosphere model (SiB) for use within general circulation models, J. Atmos. Sci., 43, 505–531, 1986.

Sellers, P. J., Randall, D. A., Collatz, G. J., et al.: A revised land-surface parameterization (SiB2) for atmospheric GCMs. Part 1: Model formulation, J. Climate, 1, 676–705, 1996a.

Stohl, A., Berg, T., Burkhart, J. F., Fjæraa, A. M., Forster, C., Herber, A., Lunder, C., McMillan, W. W. , Oltmans, S., Shiobara, M. , Simpson, D., Solberg, S., Stebel, K., Ström, J., Tørseth, K., Treffeisen, R., Virkkunen, K., and Yttri, K. E.: Arctic smoke - record high air pollution levels in the European Arctic due to agricultural fires in Eastern Europe in spring 2006,

Atmos. Chem. Phys., 7, 511–534, 2007, http://www.atmos-chem-phys.net/7/511/2007/.

Takahashi, T. S., Sutherland, S. C., Sweeney, C., Poisson, A. , Metzl, N., Tilbrook, B., Bates, N., Feely, R. A., Sabine, C., Olafsson, J., and Nojiri, Y.: Global Sea-Air CO2 flux based on climatological surface ocean pCO_2 and seasonal biological and temperature effects, Deep-Sea Res. II, 49, 1601–1622, 2002.

Vidale, P. L. and Stockli, R.: Prognostic canopy air space solutions for land surface exchanges, Theor. Appl. Climatol., 80, 245–257, 2005.

Worthy, D. E., Higuchi, K., and Chan, D.: North American influence on atmospheric carbon dioxide data collected at Sable Island, Canada, Tellus, 55B, 105–114, 2003.

Zhang, G. J. and McFarlane, N. A.: Sensitivity of climate simulations to the parameterizations of cumulus convection in the Canadian climate center general-circulation model, Atmos. Ocean, 33, 407–446, 1995.

Table 1. Description of Continuous Sites. Station ID corresponds with locations in Fig. 2.

Station ID	Station Name	Station Description
LEF	Park Falls	Northern Wisconsin; surrounded by mixed forest, wetlands, agriculture, and heavy population to the SE
FRS	Fraserdale	South of the Hudson Bay Lowland and north of the boreal forest
SGP	Southern Great Plains	Great Plains of North America in a region of strong moisture gradient, characterized by agriculture
WKT	Moody	Great Plains of North America in a region of strong moisture gradient, characterized by cattle grazing
WPL	Western Peatland	Southern boreal forest of Canada
CDL	Candle Lake	Southern boreal forest of Canada
HRV	Harvard Forest	Northeastern United States; characterized by deciduous forest and heavy population to the south
AMT	Argle	Northeastern United States; characterized by deciduous forest and heavy population to the south
TPJ	Tapajos	Tapajos National Forest in the Amazon Basin
ALT	Alert	Northeastern tip of Ellesmere Island in Nunavut, remote from major industrial regions
BRW	Barrow	Alaskan coast of the Arctic Ocean, remote from major industrial regions
PAL	Pallas	Northern Finland in the subarctic at the northern limit of the northern boreal forest zone
SBI	Sable Island	Island off the coast of Nova Scotia under influenced by anthropogenic and terrestrial airflow of North America
MHD	Mace Head	West coast of Ireland with westerly exposure to the North Atlantic Ocean
ZEP	Zeppelin	Mountain ridge in the European Arcitc off the western coast of Spitsbergen (Stohl et al., 2006)
HEI	Heidelberg	Germany, fairly strong industrial influence to the east (Gamnitzer, 2006)
HUN	Hungary	Western Hungary, flat region surrounded by agriculture and patchy forest (Haszpra, 2001)

Table 2. Annual mean percent contributions of individual terms from the PBL budget equation at AMT, CDL, SGP, and TPJ.

Station ID	Horizontal	Vertical	Cloud	Surface Flux
AMT	16%	32%	2%	50%
CDL	17%	33%	3%	47%
SGP	14%	25%	3%	58%
TPJ	4%	11%	11%	74%

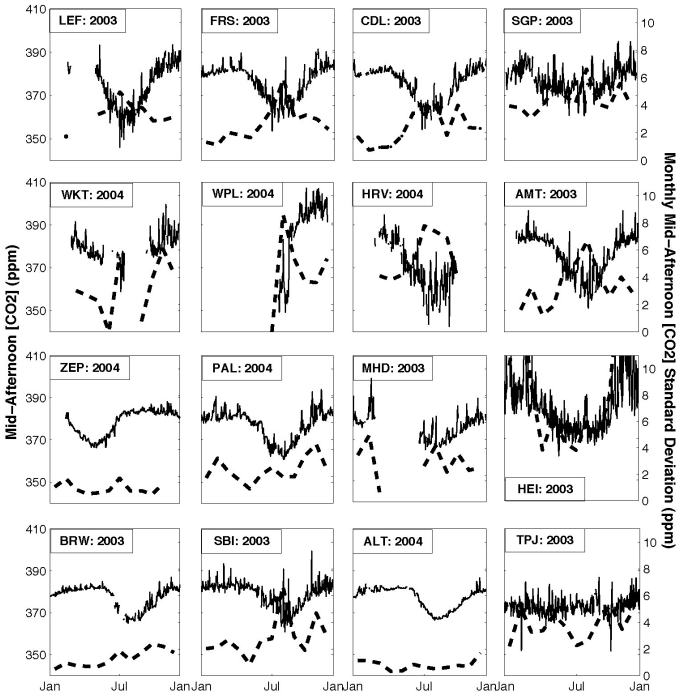

Fig. 1. Midday CO_2 (ppm) at in-situ continuous sites (solid, left y-axis) and their monthly standard deviation (dashed, right-y-axis) for 1 y.

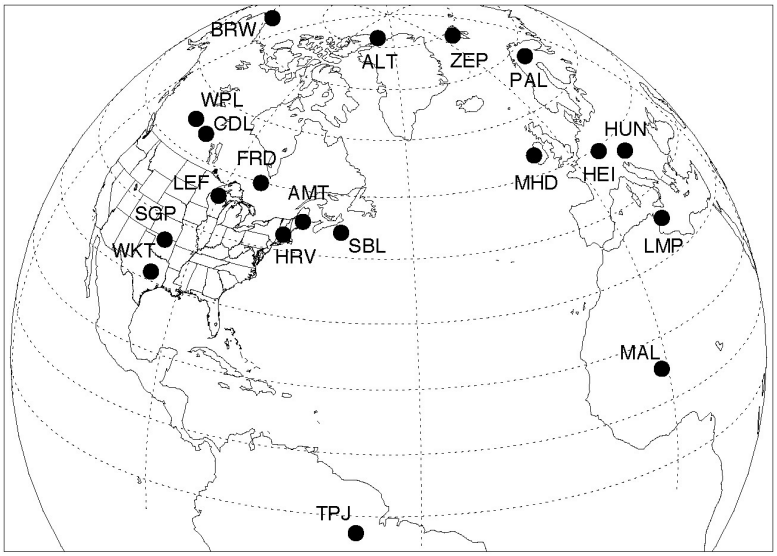

Fig. 2. Map of in-situ continuous sites.

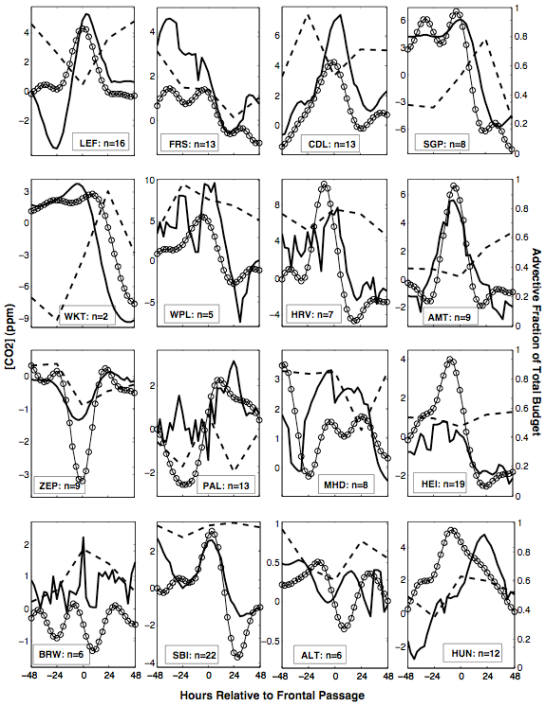

Fig. 3. (Left Y-Axis) Summer (JJA) climatology of observed (solid) and simulated (lowest model level in open circles) frontal CO_2. (Far Right Y-Axis) Total fractional contribution of daily averaged advective terms from frontal budget analysis (dashed lines). Climatologies created using method described in Sect. 3.1. The time of frontal passage is denoted by 0 on the x-axis. The station and number of events used in the averaging (*n*) is indicated within each plot.

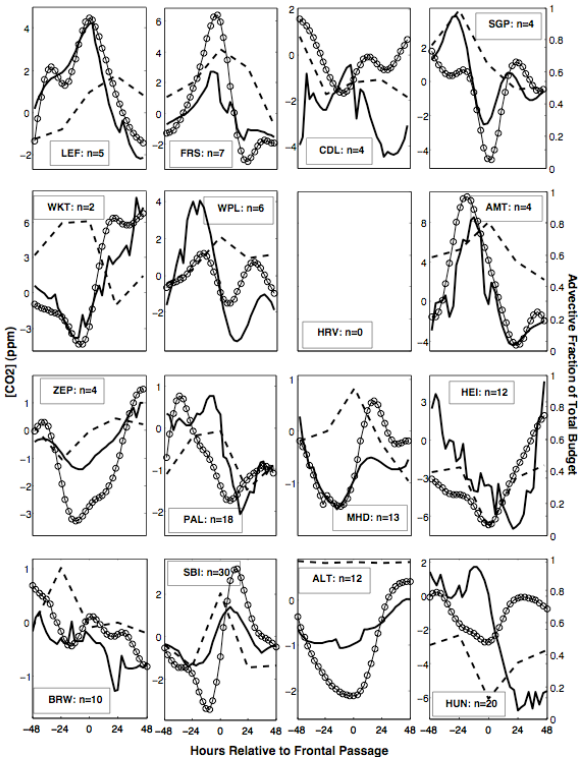

Fig. 4. Same as Fig. 3 except for Winter (DJF).

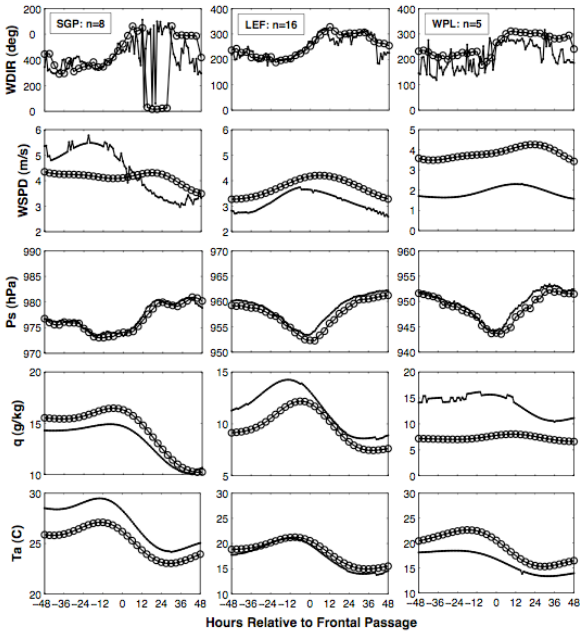

Fig. 5. Summer (JJA) climatology of observed (solid) and GEOS4-DAS (open circles) frontal weather fields at three North American sites. From top to bottom: Wind direction (WDIR) in degrees, wind speed (WSPD) in m/s, surface pressure (Ps) in hPa, specific humidity (q) in g/kg, and surface air temperature (Ta) in degrees Celsius. Observations taken at 10 m. Climatologies created using method described in Sect. 3.1. The time of frontal passage is denoted by 0 on the x-axis. The station and number of events used in the averaging (n) is indicated in the top row of plots, with each column representing the same station.

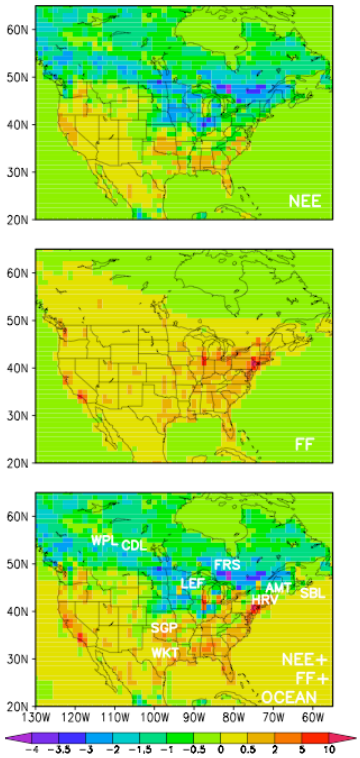

Fig. 6. July mean of hourly surface CO_2 flux of NEE (top), FF (middle), and total surface flux over land and ocean (NEE+FF+OCEAN, bottom) for North America. Each plot is on the same scale, with units of μmol/m^2/s, given by the color bar at the bottom. Locations of several continuous sites are plotted in the bottom plot for convenience.

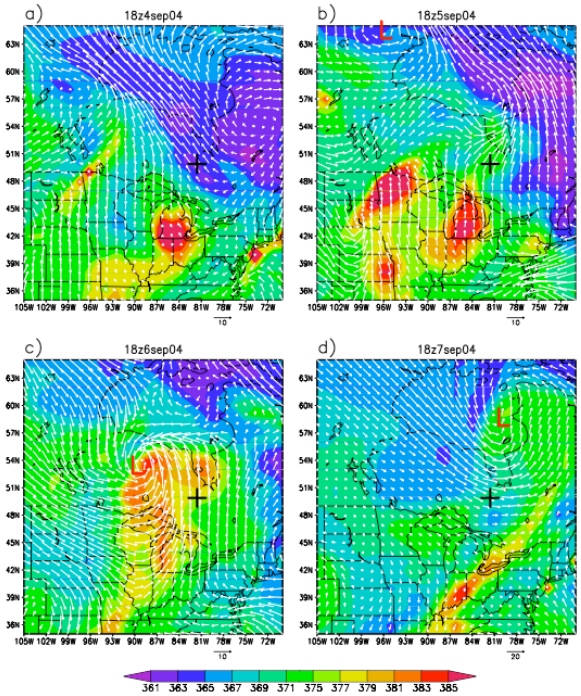

Fig. 7. Evolution of CO_2 surface anomalies (color contours) with surface winds (white vectors) as modeled over 4-day period. All times are midday (18z). The day 1 snapshot is indicated by panel **(a)**, day 2 by **(b)**, day 3 by **(c)**, and day 4 by **(d)**. The red L represents the low-pressure center of the surface cyclone migrating across the continent. The black cross indicates the location of FRS.

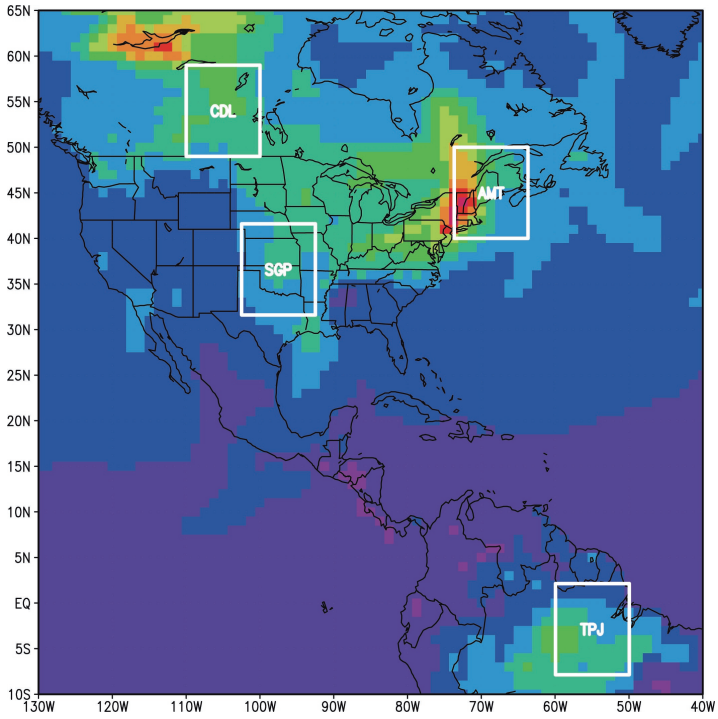

Fig. 8. Domains used for NOFLUX and NOCLOUD sensitivity experiments. Shading is example of CO_2 field at surface as simulated by PCTM.

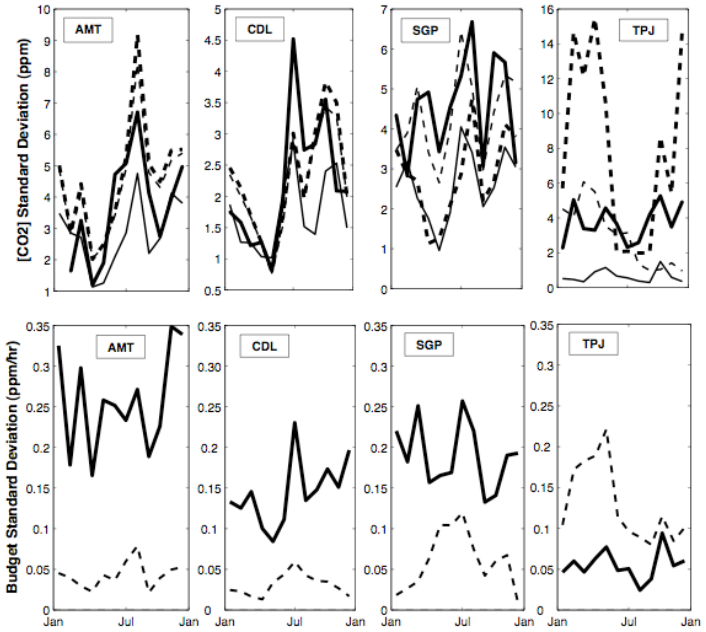

Fig. 9. (Top Row) Monthly standard deviation of midday CO_2 at grid cells containing AMT (far left), CDL (second), SGP (third) and TPJ (far right) for observations (thick solid), CONTROL (thin dashed), NOCLOUD (thick dashed), and NOFLUX (thin solid). (Bottom Row) Monthly standard deviation of horizontal advection (thick solid) and cloud transport (thin dashed) budget terms for control run.